JOURNAL OF PETROLEUM GEOMECHANICS
(JPG)

Original article

Geomechanical Study of One of Iranian Reservoirs: From Mechanical Earth Modeling to Mud Window Prediction

Amir Zargarbashi[1], Farshid Yahyaee[1], Mohammad javad Ameri[2*]

1- MSc of Petroleum Engineering, Department of Petroleum Engineering, Amirkabir University of Technology, Tehran, Iran
2- Associate Professor, Department of Petroleum Engineering, Amirkabir University of Technology, Tehran, Iran

Received: 2 November 2023; Accepted: 6 April 2024

DOI: 10.22107/JPG.2024. 423467.1215

Keywords

Wellbore Stability, Optimal Mud Weight Window, Pore Pressure, Rock Failure Criteria, Mechanical Earth Model, Drilling Problems

Abstract

Investigating the stability of the wellbore wall and controlling pore pressure and mud weight during drilling operation is one of the most important challenges that can be solved with the help of geomechanics. The existence of accurate and appropriate guidance for predicting the weight of drilling fluid and formation pore pressure is very important and can save millions of dollars annually for the industry and governments. There are different methods for calculating the mud window based on empirical relationships. In this research, a mechanical earth model (MEM) for one of the offshore reservoirs in southern Iran has been constructed and the maximum and minimum allowable drilling mud weight is presented. First, by the use of available petrophysical log data and tests, based on empirical correlations, geomechanical properties of rock were calculated and an initial guess for earth model has been prepared. Then, using additional information from daily drilling reports, final well reports, final geology reports and end of well reports (DDR, FWR, FGR, EOWR) calculated results were modified and corrected. As a result, by implementing a rock failure criterion, the optimal mud weight window has been calculated. In this research, based on the available data, the usual method of building the earth model has been modified and a mechanical earth model has tailored made for three formations. By comparing the final corrected model and the initial guess of MEM, the importance of modifying the initial guess model can be acknowledged. The prepared MEM may be used for optimizing and selecting the appropriate mud weight at the selected depth in which can reduce future drilling problems and associated risks or extend the upper limit of mud window using wellbore strengthening methods.

1. Introduction

The oil industry, like other existing industries, is always looking for ways to reduce operational costs. Among the major problems in the oil industry, stuck of the drilling string, the collapse of the wellbore due to insufficient knowledge of the geomechanical parameters of the well, formation fluid kick and loss circulation and so on can be mentioned [1]. Examining these problems and finding a way to deal with these series of problems can save billions of dollars annually. As one of the best solutions for solving these drilling problems, building a mechanical earth model is suggested. The mechanical model of the earth is a numerical modeling of the stress field and geomechanical properties of a field that is specifically defined for that field [2]. Factors such as composition, weight and pressure of the drilling mud, well trajectory, deviation and azimuth of the well are among the factors that are referred to as controllable parameters. By using the prepared model and controlling the forementioned parameters, many of the drilling problems may be prevented and mitigated.

The seamless integration of stress data, combined with the meticulously obtained in-situ

* **Corresponding Author:** Postal Code: 1591634311, Phone: +9821-66959149, ameri@aut.ac.ir

minimum horizontal stress logs previously estimated in MEM[1], adds a profound depth to the understanding of rock mechanics. Moreover, the utilization of sonic slowness and elastic shear modulus, derived from the comprehensive sonic data set, provides invaluable constraints for accurately characterizing the rock's elastic properties. This harmonious amalgamation of multidimensional data sets not only elevates the scientific rigor of the study but also unlocks new avenues for unraveling the complexities of rock behavior [3].

In studies conducted by Aghakhani Emamqeysi et al., 2022, the impact of stress variations on wellbore stability and the mud weight window was investigated. The results demonstrated that the Mogi-Coulomb criterion provides the best results, indicating complete wellbore stability. Furthermore, the transition from homogeneous to heterogeneous stress distribution leads to a reduction in the allowable maximum mud weight and increased wellbore instability [4].

In another research by Movahidnia et al., 2012, The Mohr-Coulomb, Mogi-Coulomb, and Drucker-Prager criteria were examined in well stability analysis. The Mogi-Coulomb and Drucker-Prager criteria consider the average principal stress and suggest higher shear resistance for the rock. Ultimately, in this case, more realistic results were observed using the Mohr-Coulomb criterion in the three points investigated in the well [5].

Poursiami (2013), examined different methods for calculating pore pressure using well logs and artificial neural network. Due to the unavailability of sonic travel time log for some wells, artificial neural network estimates were used, and the results showed acceptable accuracy of the estimated logs. Additionally, by comparing the calculated pore pressure values with measured data, a reasonable estimate of the actual pore pressure was obtained. It was also concluded that variations in pore pressure in different reservoirs are likely due to changes in fluid type and density [6].

In one of the oil fields in southern Iran, Rafieipour et al. have investigated the instability of the vertical wellbore wall. This instability has been attributed to the presence of shale at various depths. Therefore, to assess the stability of the wellbore wall, a linear elasticity model and a poroelasticity model have been employed. The latter model, which takes into account the effect of chemical substances closely resembling the well conditions, has higher credibility [7].

Furthermore, in one of the studies reviewed in this project, a comprehensive analysis of the wellbore stability in a field in southwest Iran has been conducted by Taherdang Kou et al. In this analysis, the most significant drilling problems, including wall collapse due to low mud weight and wellbore wall failure due to high mud weight, have been considered to examine and calculate the parameters that control wellbore stability. These parameters include rock strength, in-situ stresses, mud weight and rock properties, which highlight the importance of constructing a mechanical model for the formation [8].

There are various formulas and methods to calculate mud weight and the elastic parameters of the rock. However, the use of software is also a common approach for calculating and analyzing wellbore stability during drilling. This process has been carried out using FLAC3D software by Mirani & Habibnia, 2014. Additionally, since wellbore stability is related to the tectonic stress regime, and considering that the dominant stresses in the study area can be normal, shear, or extensional, the optimal drilling trajectory will be determined [9]. These analyses and evaluations are based on scientific and empirical foundations in the field of tectonics. For this purpose, a powerful software called "stabview" is utilized. This software is capable of providing models that suggest the best azimuth and inclination for directional drilling to drilling engineers. The aim of these recommendations is to minimize fractures in the wellbore wall [10].

In order to determine the degree of integrity of cap rocks, calculate the maximum pressure of the hydrocarbon reservoir or predict the displacement of the ground surfaces, making hydrodynamic models of hydrocarbon reservoirs is very useful and important and provides useful information regarding the mentioned options. This process includes the construction of a one-dimensional mechanical model of wells in the first stage in

[1] Mechanical Earth Model

order to calculate the geomechanical and elastic properties of the reservoir rock. During this process, Muhammad Zain-Ul-Abedin & Henk, 2020, constructed a one-dimensional mechanical earth model and calculated the elastic parameters of the rock as well as the amount of stress around the well using the data obtained from the logs. Also in later stages, a three-dimensional mechanical earth model was built using the coding method [11].

One of the main problems of drilling operations is the existence of NPT[1], which causes a huge increase in the costs of drilling operations. NPTs are due to problems such as stuck drilling pipe, collapse of the wellbore wall, formations fluid gain and loss of circulation. In order to solve these problems, which has been one of the most fundamental problems of Zubair field, using log data and drilling operation reports, Mohammed & Selman, 2020, predicted an optimal mud window for the entire well, which has resulted in huge savings in drilling operation costs [12].

In 2021, Abdulaziz et al., have also built a three-dimensional model of earth using geostatistical methods near Zubair field, which can be used to conduct a geomechanical study and analysis of the region. Construction of this 3D model, as in the previous methods, started with the construction of the mechanical earth model in one dimension. Two failure criteria of Mohr-Columb and Mogi-Columb were used in the project [13].

The study of Kidambi & Kumar, 2016, presents a comprehensive geomechanical analysis of a vertical well in a naturally fractured tight carbonate gas reservoir in the Persian Gulf. By constructing a one-dimensional mechanical earth model (MEM), the researchers gained valuable insights into the reservoir's complexities, contributing to enhanced exploration and production in challenging hydrocarbon formations [14].

The captivating study of Mursalin et al. in 2021, aims to construct a purpose-fit 1D mechanical earth model to predict injection pressure and maximum flow rate, preventing fracture growth within the reservoir. By utilizing gamma ray logs, density, compressional slowness, shear slowness, and wireline formation testers, the researchers gathered essential data. The application of the Mohr stress diagram determines the safety factor, while reservoir simulation predicts maximum water injection flow rates in inverted five-spot and inverted seven-spot patterns across three scenarios [15].

Where the presence of salt has been identified, the importance of MEM construction in order to describe drilling risks is very high. These stress perturbations are reliably mapped using MEM techniques and wellbore stability implications [16].

In research of Oruji, 2016, the instability of wellbore walls during drilling was investigated. Also, a stable path for entering the reservoir layer was introduced using a geomechanical model and different failure criteria. The results showed that the choice of failure criterion had a minimal impact on selecting the optimal path. The best drilling path in the reservoir layer was determined to be a horizontal well with a slope of 60 degrees which provided the most stability for entering the reservoir [17].

Other researches can also be mentioned in which the results are somewhat similar to results presented earlier in literature review [18], [19], [20], [21].

A complete understanding of the pre-production stress state and its changes over time plays an important role in the safe and economic operation of hydrocarbon reservoirs and underground storage sites. The instability of the internal conditions of the well is one of the main problems of the oil industry, which costs the industry about one billion dollars annually [14].

Subsurface stresses affect various operational aspects such as well stability, well integrity, stress-induced material parameter changes, fault reactivation, compression and reservoir subsidence, as well as stimulation techniques such as hydraulic fracturing.

Numerical modeling and especially mechanical earth modeling (MEM) have proven to be very valuable tool for integrating different data sets and investigating the hydromechanical response of a reservoir under different operating conditions during its life cycle. The database for such an approach (MEM) is typically derived from a wide variety of geological, geophysical, and engineering data, including field

[1] Non Productive Time

measurements, sample tests, well logs, drilling, and production data [22]. Once the numerical model is validated by calibration data such as wellbore problems and production data, it can be used to test future operational scenarios such as the stability of new wells, the optimal orientation of horizontal well paths, hydraulic fracturing, and subsidence due to pore pressure reduction ([23], [22]).

The following are among the applications of the rock mechanical model:

1. Determining the permissible mud window
2. Casing shoe selection based on pore pressure
3. Choosing the optimal drilling path

2. Gathering required data

As shown in Fig. 1. the first step to start this process is to review and collect various data, including the type of lithology, encountered drilling problems and data from petrophysical logs which are used to calculate geomechanical parameters. In this research, information such as petrophysical logs and also tests such as LOT[1], WFT[2] and DST[3] have been used. In the following, using these logs and the information extracted from them and implementing the relevant relationships, geomechanical parameters of the rock such as Young's modulus, Poisson's ratio, uniaxial compressive strength and etc. have been calculated.

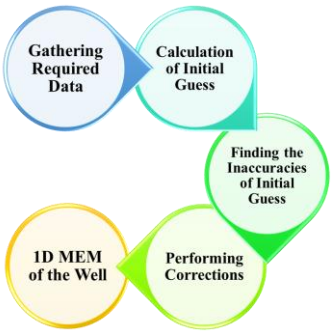

Fig. 1. Steps for preparing MEM

One of the main parts of building a mechanical earth model is gathering the required data. Most of the material required for this process is the classification of petrophysical logs taken from the desired well. By the use of existing logs and with the help of experimental correlations, initial guess for 1D earth model can be prepared step by step.

In this research, for one of the offshore reservoirs in southern Iran, studied section can be divided into three parts. The first part (Zone A) is mainly composed of mudstone, wackestone and packestone. The part in the middle (Zone B) is made up of homogeneous olive brown shale and lithology of the part at the bottom (Zone C) is mostly limestone and chalky limestone. Well azimuth varies from 207 to 211 degrees from top to bottom and variations of dip angle is between 42 to 40 degrees. Last casing shoe (9 5/8" shoe) is located at 2522 mMD[4]. Based on the available data, upper section of zone A (to about 2600 mMD) is confirmed to be oil bearing. From there below, water saturation increases significantly. Gathered petrophysical log data is shown in Fig.2. (full names are presented in Table 1).

Table 1. Full name of petrophysical logs

Name	Description
BS	Bit Size
DT	Compressional sonic log
GR	Gamma ray log
RHOB	Bulk density log
NPHI	Neutron porosity log
CALI, CALS	Caliper log
LLD	Laterolog deep
LLS	Laterolog shallow
PEF	Photoelectric factor log

3. Calculation of initial guess

The usual procedure of making a mechanical earth model is to use the forementioned gathered data and equations and follow a specific process that can be used to determine the mud window using empirical equations. This stage is the initial part of the research and the initial model should be modified for more validity.

3.1. Shear and compressional slowness logs

In order to calculate the shear velocity, in the absence of DSI[5] log, various empirical relations

[1] Leak Off Test
[2] Wireline Formation Testers
[3] Drill Stem Test
[4] Measured Depth
[5] Dipole Shear Sonic Imager

such as Christensen's equation can be used. According to the available data, Christensen's experimental method has been used in this article ([1],[22]).

$$V_s = V_p \left[1 - 1.15 \left(\frac{\frac{1}{\rho} + \frac{1}{\rho^3}}{e^{\frac{1}{\rho}}} \right)\right]^{3/2} \quad (1)$$

In which V_s is shear wave velocity, V_p is compressional wave velocity and ρ is the bulk density of formation rock. The results of calculating the velocities using the empirical relationship (in the format of compressional and shear slowness) are shown in Fig. 3.

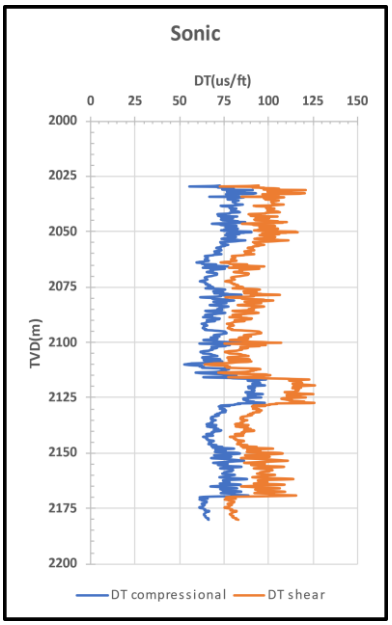

Fig. 3. Shear and compressional slowness

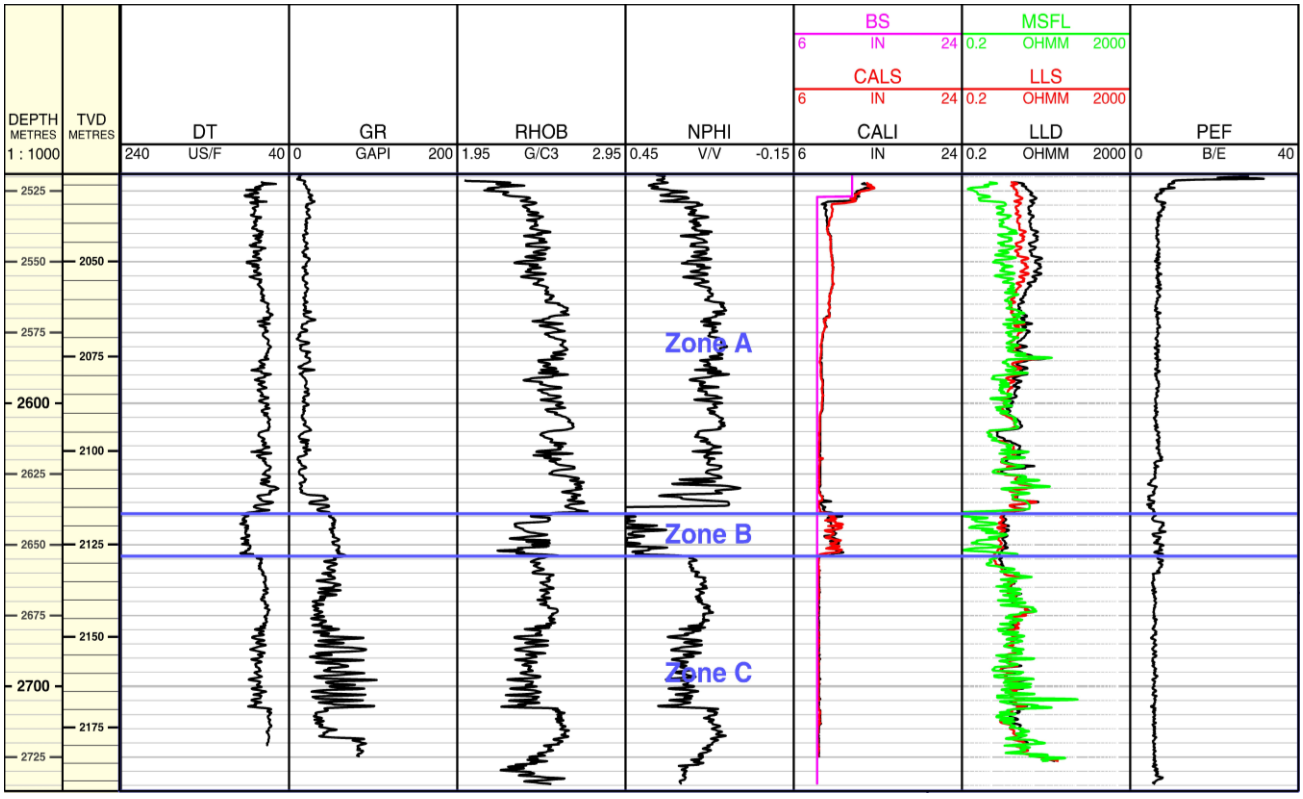

Fig. 2. Available petrophysical logs

3.2. Bulk density and overburden pressure

Since the bulk density log (RHOB) is typically recorded only at deeper intervals, this info is unavailable from the surface. Amoco equation which is presented in equation (2) is used to construct a model for the prediction of density in the area where RHOB logging data is not available. Calculating the bulk density is generally not particularly complicated and it is possible to link density and depth (TVD[1]) together using a valid empirical formula and calculate the constant parameters of the equation (ρ_0, a, b) and calculate the density for various other points (equation 3). This method has been tested in this section and the result can be seen in the diagram below [24].

$$\rho = \rho_0 + a\,TVD^b \quad (2)$$

$$\rho = 1.95 + 0.03517 \times TVD^{0.3522} \quad (3)$$

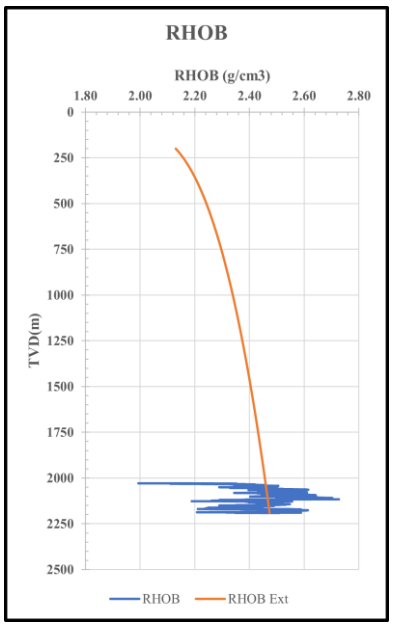

Fig. 4. Extrapolated density log data

By performing an integral over the extrapolated bulk density values, overburden pressure (σ_v) can simply be calculated using the following equation.

$$\sigma_v = \int_{TVD_{mudline}}^{TVD_{TD}} \rho g(TVD) + P_{Sea\ water} \quad (4)$$

By using the water depth and density of sea water, $P_{Sea\ water}$ can be easily calculated. For the density of sea water, the value of 8.585 ppg was considered [25].

3.3. Young's modulus and Poisson's ratio

The dynamic Poisson's ratio is calculated using the following equation [26, 27].

$$\nu_{dynamic} = 0.5\,\frac{V_p^2 - 2V_s^2}{V_p^2 - V_s^2} \quad (5)$$

$$\nu_{static} = 0.7\nu_{dynamic} \quad (6)$$

Where V_s is shear wave velocity and V_p is compressional wave velocity. The subscript dynamic used in these equations indicates that these are dynamic properties as they refer to the properties of the rock at sonic velocities and frequencies of around 10 kHz. In this situation, the strain is not as high as that of mechanical tests in the lab. Therefore, dynamic parameters obtained from these equations are overestimated values and need to be converted to static properties through an empirical correlation. Poisson's ratio in dynamic and static mode is plotted in Fig.5.

Young's modulus is one of the most important elastic properties that can be calculated using sonic and density logs. Eissa and Kazzi correlation is used to estimate the static Young's modulus [27]:

$$G_{shear} = 1.34 \times 10^4 \times \frac{\rho}{\Delta t_s^2} \quad (7)$$

$$E_{dynamic} = 2G_{shear}(1 + \nu_{dynamic}) \quad (8)$$

$$E_{static} = 0.74E_{dynamic} - 0.82 \quad (9)$$

In which Δt_s is the shear sonic log data, and $E_{dynamic}$ and E_{static} are dynamic and static Young's modulus respectively.

[1] Ture Vertical Depth

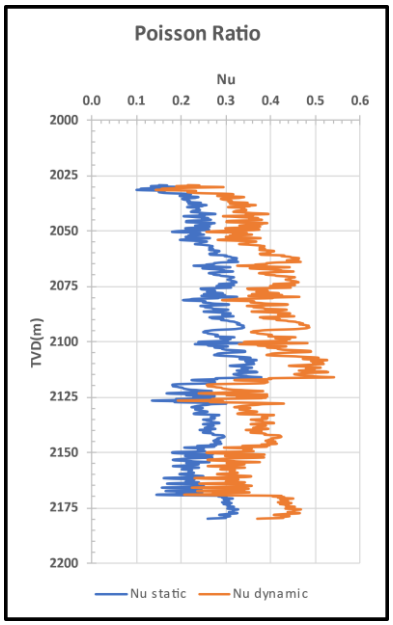

Fig. 5. Static and dynamic poisson's ratios

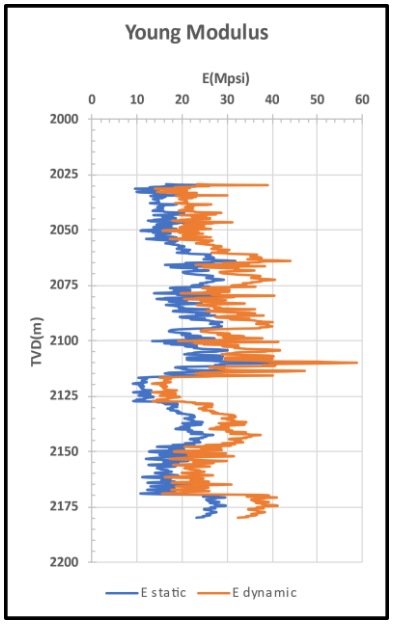

Fig. 6. Static and dynamic Young's modules

3.4. Uniaxial compressive strength (UCS) of the rock

This parameter can be determined directly in the laboratory by performing uniaxial or triaxial tests on core samples taken from the desired depth. However, in many cases, accessing the core samples of the rock for testing is not possible. Therefore, a number of empirical correlations have been proposed to relate rock strength to borehole measurements.

This rock property is generally dependent on the rock type and for each lithology, there are different empirical formulas. Correlations used in this study are listed in Table 2 [28].

Table 2. UCS based on rock types

Correlation	Rock type	Reference
$195.8 \times \left(\frac{304.8}{\Delta t_p}\right)^{2.6}$	Shale	[29]
$10^{(2.44+\frac{109.14}{\Delta t_p})}$	Limestone	[30]
$40847e^{-0.0268\Delta t_p}$	Sandstone	[31]
$111.68 \times \left(\frac{304.8}{\Delta t_p}\right)^{2.93}$	Marl	[31]

Based on the lithologies encountered in this article, the first two equations were used to calculate UCS. Results are plotted in Fig. 7.

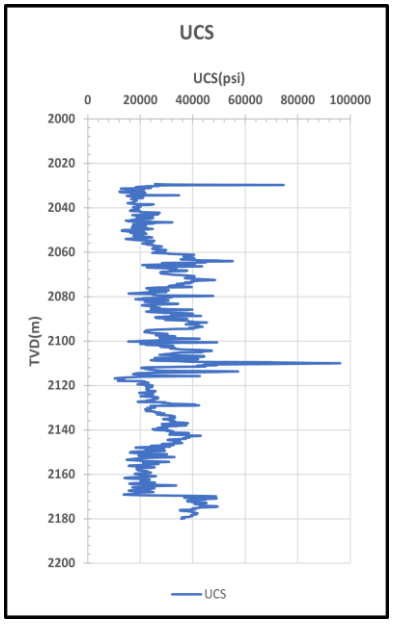

Fig. 7. Predicted UCS values

3.5. Shale Fraction and Porosity

To estimate the shale fraction, Plumb's correlation is one of the best empirical correlations. In general, as mentioned in the previous sections,

one of the main criteria for using any experimental formula is to check the available data [32]. To compensate for the erroneous peaks in gamma ray log, an average value is considered for GR_{max} and any calculated shale volume (V_{shale}) larger than 1 are disregarded. Minimum value of gamma ray log is used as GR_{min}.

$$V_{shale} = \frac{GR_{log} - GR_{min}}{GR_{max} - GR_{min}} \quad (10)$$

For the value of porosity, total porosity log data (which can be obtained by NPHI log interpretation) is used. Results can be seen in Fig.8.

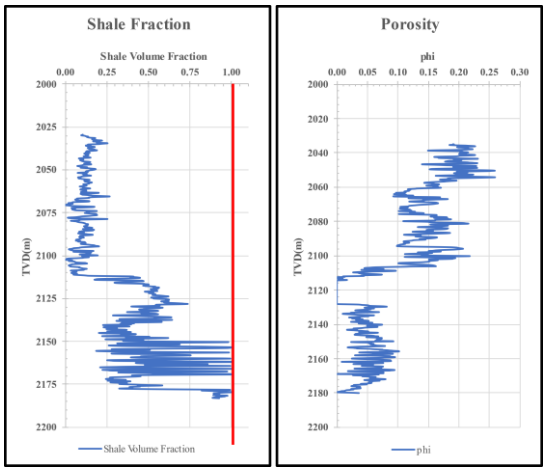

Fig. 8. Shale fraction and porosity log data

3.6. Friction angle

Because of the complex relationships between friction angle (φ) and rock geomechanical properties, few attempts have been made to establish relationships between friction angle and well log data. Nevertheless, it has been shown through experimental studies that with the increase of Young's modulus, the value of the friction angle also increases. However, based on the studies for this field, Plumb's empirical relation (equation (11)) has been used [32].

$$\varphi = 26.5 - 37.4(1 - \Phi - V_{shale}) + 62.1(1 - \Phi - V_{shale})^2 \quad (11)$$

In which φ is the calculated friction angle, V_{shale} is the volume of shale, and Φ is porosity of the rock. Erroneous values are filtered in Fig. 9.

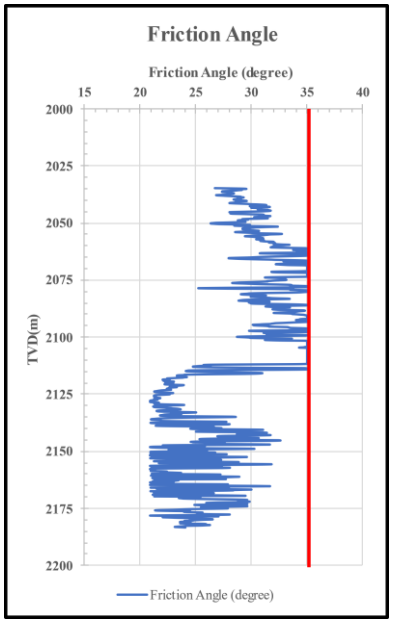

Fig. 9. Calculated and corrected friction angles

3.7. Pore pressure

To calculate the pore pressure, which is one of the most important design parameters of the drilling operation program, the pressure points measured using wireline formation tester (WFT) tools can be used. But in this case, due to the lack of WFT measurements for all of the section interval, Eaton's empirical formula has been used as an alternative. This correlation is as follows [33].

$$PPG = OBG - (OBG - PPN) \times 1 \times \left(\frac{\Delta t_{normal}}{\Delta t_p}\right) \quad (12)$$

In this equation, several variables are used including OBG[1] as the overburden pressure gradient, PPN[2] as the pressure gradient caused by normal pore pressure (which in this case, based on sea water salinity, could be considered as 0.446 [25]), Δt_p as the compressional sonic wave slowness, and Δt_{normal} is a trend line that fits on a specific part of the sonic log chart. By using these parameters, PPG or pore pressure gradient can be calculated.

To use this correlation, the first step is to fit a normal trend line on sonic log data, which is shown in Fig.11. Four different lines were fitted

[1] Overburden Gradient

[2] Normal Pore Pressure Gradient

and their equations were extracted (each part is shown with a specific title color in Fig. 11). These trend line equations were then used in equation (12) to calculate pore pressure using the Eaton correlation. The results are depicted in Fig. 10.

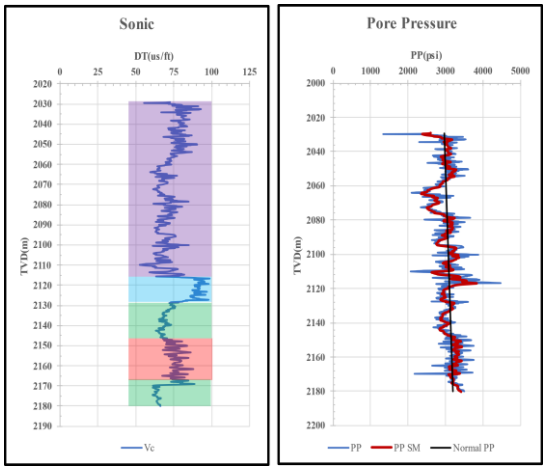

Fig. 10. In the left, Sonic log is divided into for zones (purple, blue, green, red) and in the right, calculated pore pressure is presented (SM stands for smoothed)

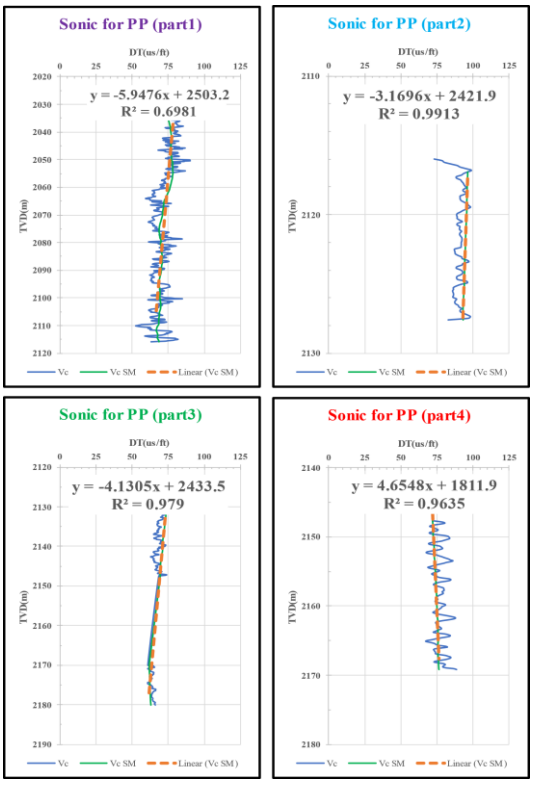

Fig. 11. Sonic log trend line zones and equations

3.8. In-situ Stresses

This study uses the poro-elastic horizontal strain model to calculate the minimum and maximum horizontal stresses. Formulation of the model is expressed as follows ([14], [34], [35]):

$$\sigma_h = \left(\frac{\nu}{1-\nu}\right)(\sigma_v - \alpha P_p) + \alpha P_p + \frac{E_s}{1-\nu^2}(\varepsilon_x + \nu\varepsilon_y) \quad (13)$$

$$\sigma_H = \left(\frac{\nu}{1-\nu}\right)(\sigma_v - \alpha P_p) + \alpha P_p + \frac{E_s}{1-\nu^2}(\varepsilon_y + \nu\varepsilon_x) \quad (14)$$

Equations (13) and (14) involve the strains ε_x and ε_y, which represent the deformation of rock in the x and y planes, respectively. These strains are calculated as functions of the overburden stresses [4,7]:

$$\varepsilon_x = \frac{\sigma_v \nu}{E_s}\left(\frac{1}{1-\nu} - 1\right) \quad (15)$$

$$\varepsilon_y = \frac{\sigma_v \nu}{E_s}\left(1 - \frac{\nu^2}{1-\nu}\right) \quad (16)$$

The results of utilizing equations (15) and (16) to calculate the minimum and maximum in-situ horizontal stresses of σ_h and σ_H (equations (13) and (14)) are presented in Fig. 12 And Fig. 13, respectively.

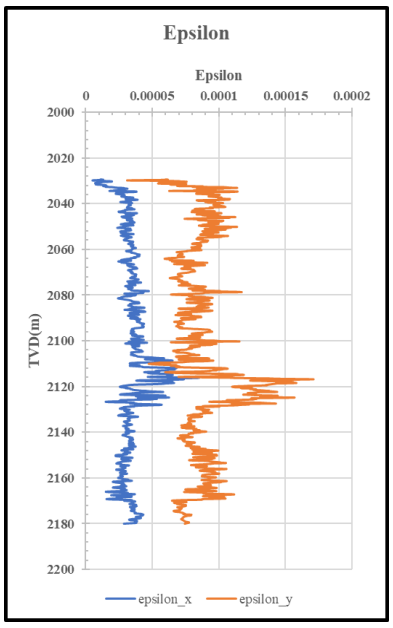

Fig. 12. Initial guess of horizontal strains in x and y direction

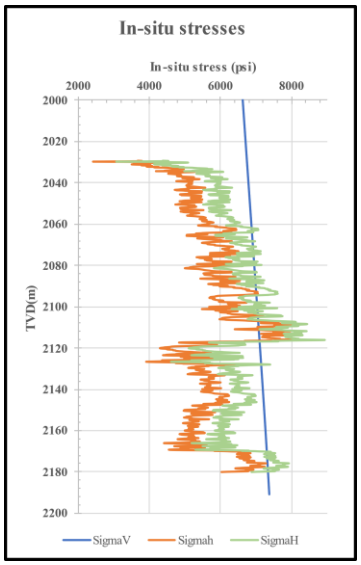

Fig. 13. Initial guess of in-situ stresses (and overburden pressure)

3.8. Wellbore stability and initial mud window

In this section, the goal of determining the initial mud weight window is achieved by calculating the breakout and pore pressure gradient (which represents the lower limit of mud window) and the fracture pressure gradient (which represents the upper limit of mud window) using estimated geomechanical properties. The Mogi-Coulomb criterion is used as the failure criterion for these calculations.. Mogi (1971) proposed a failure criterion for brittle failure under multiaxial stress states, stating that failure always occurs along a plane aligned with the principal intermediate stress direction. As such, the following failure criterion has been proposed:

$$\tau_{oct} = f(\sigma_{m,2}) \quad (17)$$

The failure criterion provided by Mogi consists of a non-linear power law function denoted by f. The effective mean stress is denoted by $\sigma_{m,2}$, while the octahedral shear stress is denoted by τ_{oct}.

$$\sigma_{m,2} = \frac{\sigma_1+\sigma_3}{2} \quad (18)$$

$$\tau_{oct} = \frac{1}{3}\sqrt{(\sigma_1-\sigma_2)^2+(\sigma_1-\sigma_3)^2+(\sigma_2-\sigma_3)^2} \quad (19)$$

The parameters of the Mogi failure function, cannot be directly related to the Coulomb power parameters c and φ. To address this issue, Al-Ajmi suggested that the function f can be approximated as a linear function, which is expressed as follows [36]:

$$\tau_{oct} = a + b\sigma_{m,2} \quad (20)$$

$$a = \frac{2\sqrt{2}}{3} c \times cos(\varphi) \quad (21)$$

$$b = \frac{2\sqrt{2}}{3} c \times sin(\varphi) \quad (22)$$

Equation (20) represents the Mogi-Coulomb failure criterion, which extends Coulomb's linear criterion to the Mogi stress domain. By applying the Mogi-Coulomb law, the reinforcing effect of the intermediate principal stress can be taken into account. The first and second stress variables, I_1 and I_2, are defined as below:

$$I_1 = \sigma_1 + \sigma_2 + \sigma_3 \quad (23)$$

$$I_2 = \sigma_1\sigma_2 + \sigma_1\sigma_3 + \sigma_2\sigma_3 \quad (24)$$

When utilizing the Mogi-Coulomb criterion, the following can be inferred:

$$\sqrt{I_1^2 - 3I_2^2} = a' + b'(I_1 - \sigma_2) \quad (25)$$

Where:

$$a' = 2c \times cos(\varphi) \quad (26)$$

$$b' = sin(\varphi) \quad (27)$$

The first and second stress invariants are as follows:

$$I_1 = D + E \quad (28)$$

$$I_2 = DE + DP_W - P_W^2 \quad (29)$$

To determine the mud pressures corresponding to the lower bounds of mud weight window we will act based on the following conditions [37].

$\sigma_1 \geq \sigma_2 \geq \sigma_3$ wellbore failure will occur if $P_W \leq P_{W(BO)}$

$\sigma_z \geq \sigma_\theta \geq \sigma_r$ $P_{W(BO)} = \frac{1}{6-2b'^2}\left[(3A + 2b'K) - \sqrt{H + 12(K^2 + b'AK)}\right]$

$\sigma_\theta \geq \sigma_z \geq \sigma_r$ $P_{W(BO)} = \frac{1}{2}A - \frac{1}{6}\sqrt{12\left(a' + b'(A - 2P_p)\right)^2 - 3(A - 2B)^2}$

$\sigma_\theta \geq \sigma_r \geq \sigma_z$ $P_{W(BO)} = \frac{1}{6-2b'^2}\left[(3A - 2b'G) - \sqrt{H + 12(G^2 - b'AG)}\right]$

where

$$A = 3\sigma_H - \sigma_h \quad (30)$$

$$B = \sigma_v + 2\nu(\sigma_H - \sigma_h) \quad (31)$$

$$H = A^2(4b'^2 - 3) + (B^2 - AB)(4b'^2 - 12) \quad (32)$$

$$K = a' + b'(B - 2P_p) \quad (33)$$

$$G = K + b'A \quad (34)$$

Mogi-Coulomb criterion for determination of breakdown pressure is as follows [37].

$\sigma_1 \geq \sigma_2 \geq \sigma_3$ wellbore breakdown will occur if $P_W \geq P_{W(frac)}$

$\sigma_r \geq \sigma_\theta \geq \sigma_z \quad P_{W(frac)} = \frac{1}{6-2b'^2}\left[(3D + 2b'N) + \sqrt{J + 12(N^2 + b'DN)}\right]$

$\sigma_r \geq \sigma_z \geq \sigma_\theta \quad P_{W(frac)} = \frac{1}{2}D + \frac{1}{6}\sqrt{12\left(a' + b'(D - 2P_p)\right)^2 - 3(D - 2E)^2}$

$\sigma_z \geq \sigma_r \geq \sigma_\theta \quad P_{W(frac)} = \frac{1}{6-2b'^2}\left[(3D - 2b'M) + \sqrt{J + 12(M^2 - b'DM)}\right]$

where:

$$D = 3\sigma_h - \sigma_H \quad (35)$$

$$E = \sigma_v - 2\nu(\sigma_H - \sigma_h) \quad (36)$$

$$J = D^2(4b'^2 - 3) + (E^2 - DE)(4b'^2 - 12) \quad (37)$$

$$N = a' + b'(E - 2P_p) \quad (38)$$

$$M = N + b'D \quad (39)$$

The dip and azimuth of the well have been considered and the Mogi-Coulomb criterion has been applied to obtain breakout and breakdown values. It is important to note that the obtained mud weight window (Fig. 14) is only a preliminary guess and will be used in the next sections to build the MEM model, but it is not the final result.

4. Finding the inaccuracies of initial guess

After building the initial numerical model, for further validation, the results of the model should be evaluated with well data. After finding all the inaccuracies, corrections will be made in the next section.

4.1. Inaccuracies of pore pressure diagram

In next two subsections, calculated pore pressure diagram, will be examined by the use of WFT and DST test results and also by checking against the gain reports.

4.1.1. Pore pressure vs WFT and DST

48 WFT data points were available for this well. After disregarding failed and supercharged samples, the results were used to validate the Eaton proposed pore pressure gradient. In addition to WFTs, two DSTs were conducted in lower and upper sections of zone A (see Fig. 2), and their results were also used for validation.

Fig. 15 shows a difference between the actual pore pressure values obtained from WFT and DST and the predicted value from Eaton correlation, as highlighted in the figure.

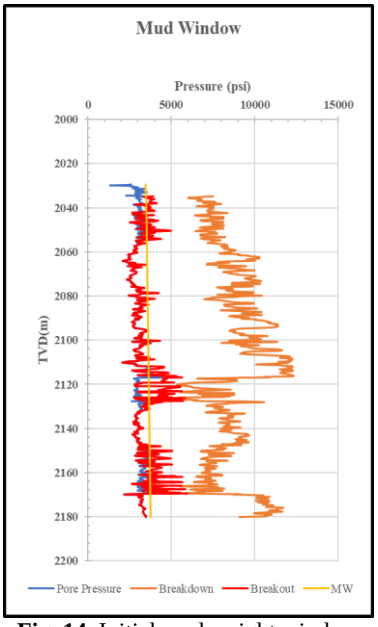

Fig. 14. Initial mud weight window

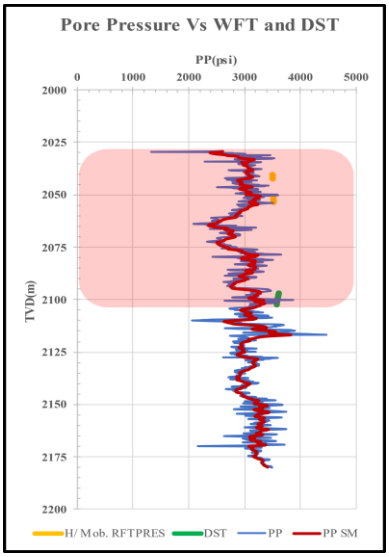

Fig. 15. Inaccuracies of proposed PP vs WFT and DST data (SM stands for smoothed)

4.1.2. Pore pressure vs gain reports

According to DDR[1]s, while the gain reports indicate a continuous gas gain from 2028 to 2118 mTVD (throughout the zone A), the predicted pore pressure is actually lower than the mud weight used during drilling of this section (Fig. 16). This contradicts the nature of a gain, where the mud pressure exerted is less than the pore pressure, allowing formation fluid to enter the wellbore.

4.2. Inaccuracies of breakout diagram

The caliper log is one of the most effective tools for evaluating the predicted breakout value using the Mogi-Coulomb criterion. If borehole failure is solely the result of the stress field around the wellbore wall and not affected by other factors such as the nature of the rock (e.g., sloughing and swelling shale that tends to absorb drilling fluid and break into the borehole), the caliper log can be used to verify the predicted breakout. Fig. 17 shows the breakout and caliper log data plotted side by side. Highlighted sections, indicate the areas in which breakout prediction model, doesn't match with the actual caliper data. For example, the blue highlight shows borehole failure between 2150 m and 2170 m, despite no visible sign of failure in caliper data.

4.3. Inaccuracies of breakdown diagram

Breakdown values should be evaluated using LOT results and loss reports.

4.3.1. Breakdown vs LOT

To evaluate the predicted breakdown values, the recorded LOT result at 2067 mTVD was used. This LOT was performed after entering the 8 1/2" section and near the 9 5/8" casing shoe, and a value of 4450 psi was recorded. Fig. 18 compares this value with the predicted breakdown trend.

4.3.2. Breakdown vs loss report

Finally, the breakdown values were compared to the recorded loss reports. Based on DDRs, one interval of loss circulation has been recorded in this section, and the breakdown values need to be corrected to match this loss report. Comparison is plotted in Fig. 19.

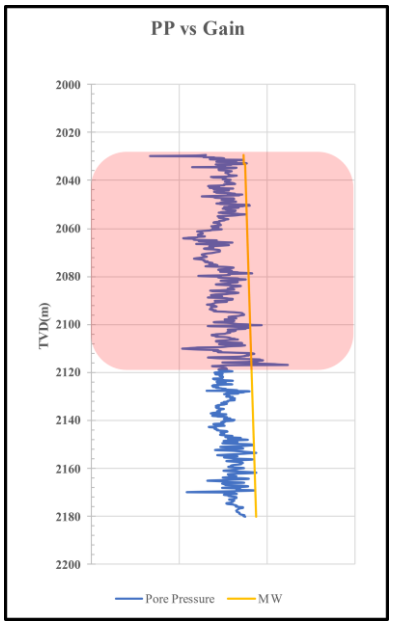

Fig. 16. Inaccuracy of predicted pore pressure vs gain reports

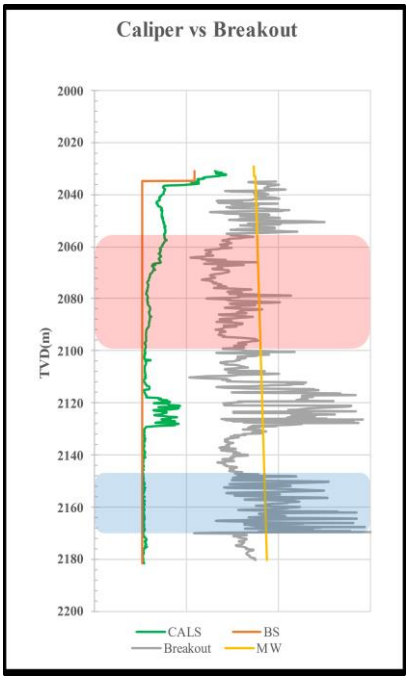

Fig. 17. Inaccuracies of calculated breakout vs caliper log

[1] Daily Drilling Report

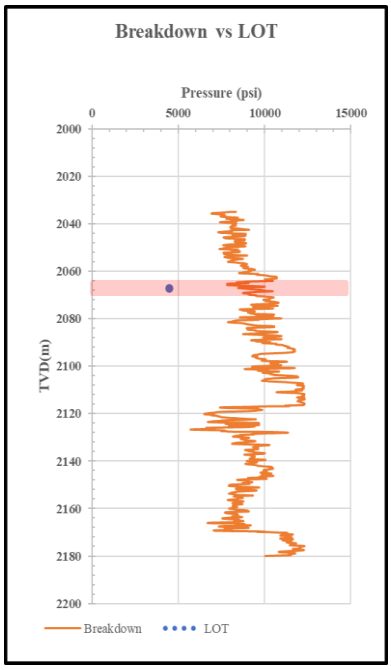

Fig. 18. Predicted breakdown vs LOT

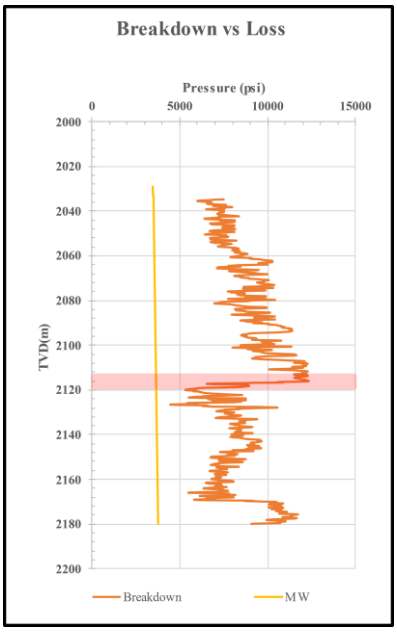

Fig. 19. Predicted breakdown vs loss reports

5. Corrections of initial guess

In general, to increase the validity of the constructed numerical model, the model should be validated with the conducted experiments to accommodate the special conditions in which, cannot be predicted and described with a numerical model. For this purpose, FWR[1], EOWR[2], FGR[3] and DDRs will be used to detect these errors and inaccuracies.

The initial guess of the MEM model has been corrected in three parts. It is important to apply these modifications in the order they are presented, as the items are interdependent. It is not possible to attempt to correct an item before addressing the item it is dependent on. Three parts are included in the corrections of the initial guess of the MEM model, which are:

1. Pore pressure correction
2. ε_x and ε_y correction
3. UCS correction

5.1. Pore pressure correction

To correct for pore pressure, Eaton correlation output was calibrated with WFT and DST data. This calibration was performed only in the specific formation, because these data were only available in forementioned interval. The calibration results are presented in Fig. 20. As shown in the left side of Fig. 20, predicted pore pressure values from Eaton correlation doesn't match with the actual WFT and DST data. A solid black line is overlayed on the WFT and DST data to find the actual pore pressure trendline of this section. This part of pore pressure trend is shifted to match the solid line trend and the result is shown in the right diagram of Fig. 20.

By applying this calibration, part of the inaccuracy shown in Fig. 16 (for comparison with gain reports) is also resolved. This continuous gas show was reported during drilling of this section (about 120m interval) and to completely accommodate this gas gain, another calibration is needed which is shown in Fig. 21.

Fig. 22 shows the corrected pore pressure and its effect on the value of predicted breakout. As can be seen (Left diagram is same as Fig.17 and is plotted using initial guess of pore pressure; right diagram is plotted using corrected pore pressure), one of the problems in predicted value of breakout

[1] Final Well Report
[2] End of Well Report
[3] Final Geological Report

(red highlight in Fig. 22.) is resolved.

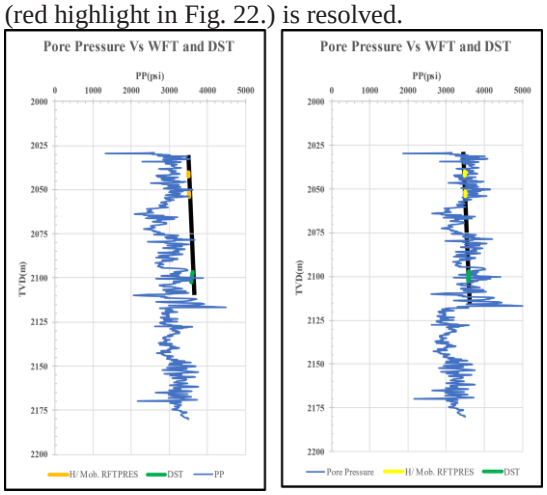

Fig. 20. Correction of pore pressure with WFT and DST reports

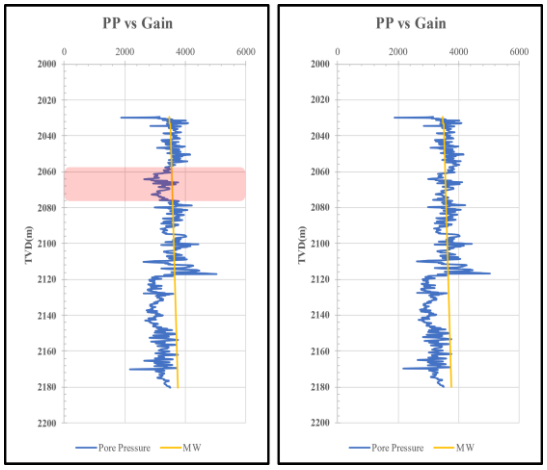

Fig. 21. Pore pressure calibration with gain reports

5.2. ε_x and ε_y correction

The second step in performing the corrections involved correcting the value of strains, which in turn corrected the breakdown value. To accomplish this, the LOT result at 2067 mTVD was used, and the values of strains (ε_x and ε_y) were adjusted in such a way that the new values of in-situ stresses, resulted in a breakdown value close to LOT result (around 4450 psi) at the test point. Results are presented in Fig. 23.

By applying these corrections, the calibrated curve, also matches the loss report presented in Fig. 19 (partial loss that reported in around 2120 mTVD). The following figure (Fig. 24) presents this corrected plot.

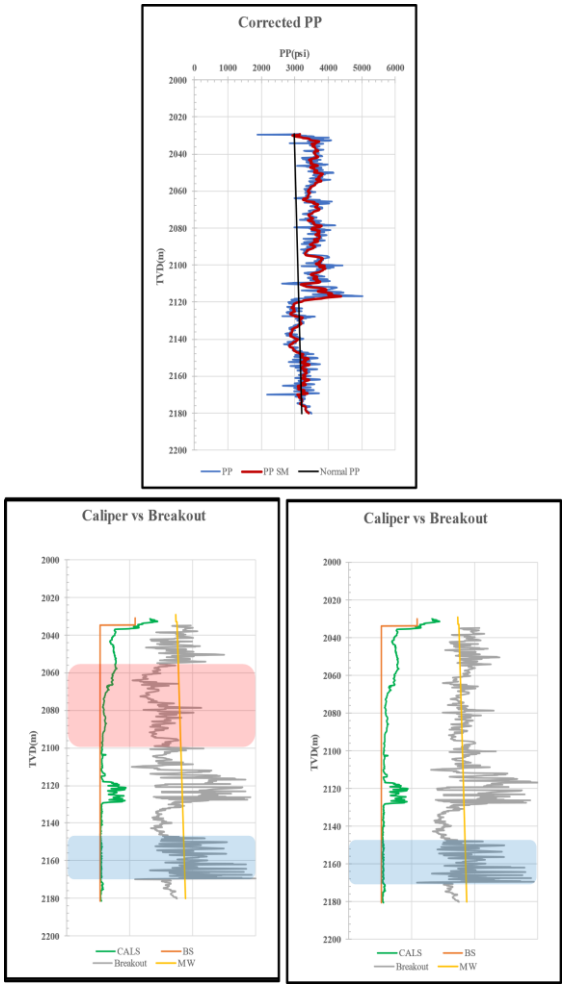

Fig. 22. Corrected pore pressure (top diagram), effect of PP change on predicted breakout plot (left diagram is plotted using initial guess of PP and the right diagram shows the effect of corrected PP values on breakout calculation)

5.3. UCS correction

The final step in making corrections involves calibrating the UCS value. Using caliper log data and the Mogi-Coulomb criterion, the actual UCS values at the breakpoints were calculated. Based on lithology, a correction factor for each lithology and formation type was then determined (by dividing the actual value by the estimated UCS value at the breakout points). Using this correction factor, the UCS value of each lithology type and each zone was calibrated and the final results are

plotted in Fig. 25. The effect of this modification on the calibrated breakout values is also shown in Fig. 25. By performing this modification, all the problems associated to the initial guess of breakout values (blue highlight in Fig. 22) were solved. It should be noted that the breakout in zone B (about 2115 to 2130 mTVD) is the result of sloughing and swelling shales in this area and because of that, its effect can't be seen in corrected breakout values.

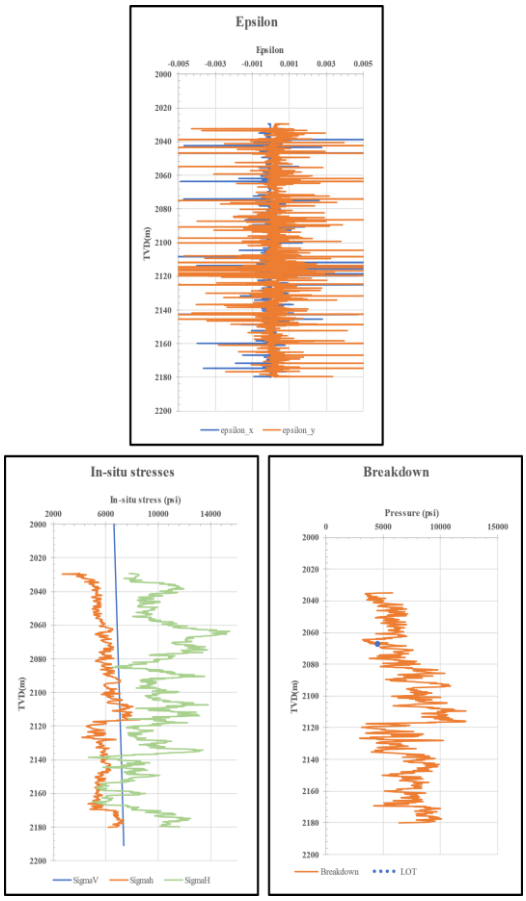

Fig. 23. Corrected (calibrated) strains (top), corrected in-situ stresses (left) and corrected breakdown value (right) using LOT result

5.4. Final mud weight window

After all the mentioned corrections, the final mud window is presented in Fig. 26. This figure shows the range of optimized mud weights that can be used to safely drill a well without encountering drilling hazards such as well instability, loss circulation or well flow and stuck pipe. By staying within the optimized mud weight range, the drilling program can continue with greater confidence and efficiency, ultimately leading to successful well completion. Final corrected in-situ stresses are also presented in Fig. 27.

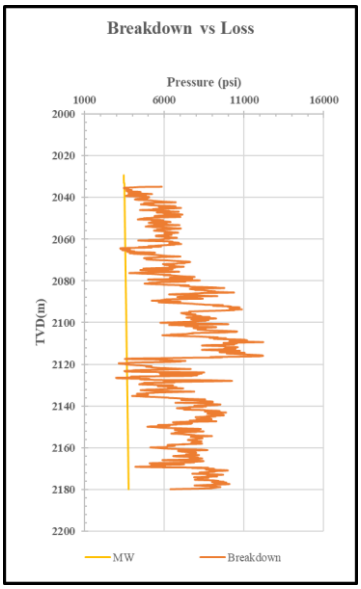

Fig. 24. Corrected breakdown matches with reported loss circulation interval

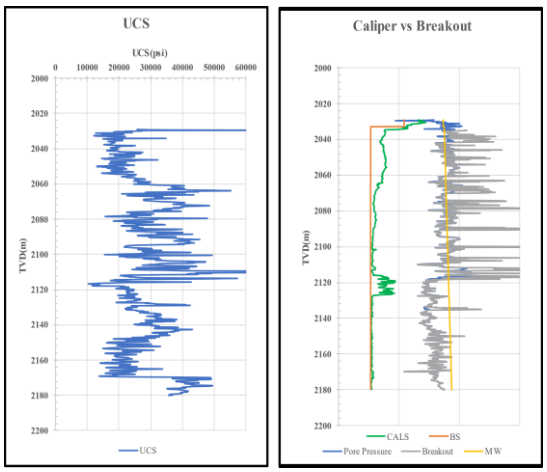

Fig. 25. Corrected UCS and its effect on breakout

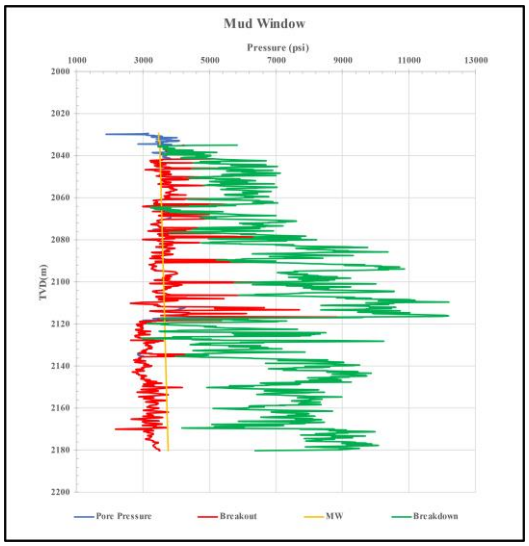

Fig. 26. Final Mud Window

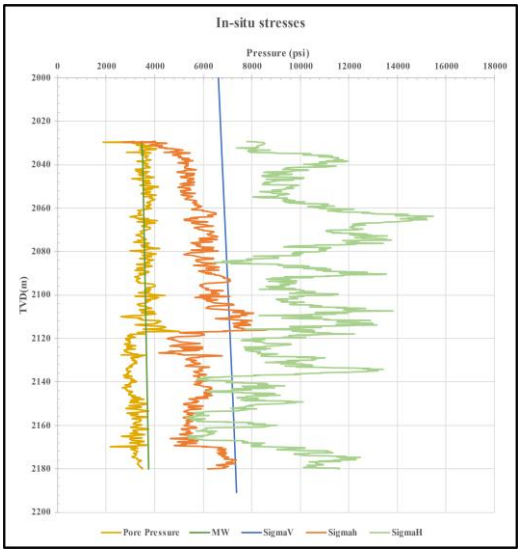

Fig. 27. Final in-situ stresses

6. Conclusions

Drilling problems can have a significant impact on the drilling schedule and overall, well success. It is therefore very important that these problems are accurately reported during drilling operations and mitigated in future drilling programs. This data provides valuable information that can be used during the construction of a MEM (mechanical earth model), which is a detailed description of the subsurface conditions encountered during drilling. MEM is used to optimize drilling parameters such as mud weight, drilling speed, bit selection, and to identify potential hazards such as well instability, loss of circulation or well flow and stuck pipe. By accurately reporting drilling problems and using them to build MEMs for different wells of a developing field, the drilling program can be managed more effectively.

In general, the results are as follows:

1. In this research, the usual method of building the mechanical earth model was modified and based on the available data, the procedure was tailor made for this well.
2. As shown in this research, by comparing the final corrected model and the initial guess of MEM, the importance of modifying the initial guess model can be acknowledged.
3. In this project a new form of Eaton correlation (using four different trend lines) is used to estimate pore pressure using compressional sonic log data. Results show the applicability and high accuracy of this method.
4. As can be seen in the forementioned sections, the importance of data collection during drilling operations is highlighted. Every collected data may be used in some way for the future development of the field.
5. Using tests like FIT[1] and LOT help researchers to correct the maximum and minimum horizontal stress levels. Although it might be expensive to perform some of these tests, the results are valuable enough to justify the costs.
6. Experimental methods using cores are the most accurate methods to determine the geomechanical parameters of rocks. Measuring geomechanical properties of core samples helps researchers to correct the results of calculated MEM accurately. Also, interdependently, the results of MEM construction may be used to indicate the initial condition for some core experimental test.
7. The prepared mud window may be used for optimizing and selecting the appropriate mud weight at the selected depth, optimize casing shoe placement and drilling path or extend the upper limit of mud window using wellbore strengthening methods.
8. One of the other uses of MEM is the identification of stress regim in the area. The

[1] Formation Integrity Test

stress model indicates that the stress regime is between strike-slip and normal. Dominant stress regime is strike-slip and in some sections it changes to normal.

7. Reference

[1] Humand, M., & Ameri, M. J. (2018). Constructing a mechanical earth model and determining the optimal mud window for the Belal field 3rd National Petroleum Geomechanics Conference, https://civilica.com/doc/923138

[2] Afsari, M., Ghafoori, M., Roostaeian, M., Haghshenas, A., Ataei, A., & Masoudi, R. (2009). Mechanical earth model (MEM): An effective tool for borehole stability analysis and managed pressure drilling (case study). SPE Middle East Oil and Gas Show and Conference,

[3] Wendt, A. S., Kongslien, M., Renlie, L., Pedersen, E. S., Vissapragada, B., Skomedal, E., & Sinha, B. K. (2007). Advanced mechanical earth modelling and wellbore-stability calculation using advanced sonic measurements: A case study on an HP/HT field in the Norwegian North Sea. SPE Annual Technical Conference and Exhibition,

[4] Aghakhani Emamqeysi, M. R., Fatehi Marji, M., Hashemizadeh, A., Sanei, M., & Abdollahipour, A. (2022). 3D Numerical modeling of the effect of in-situ stress ratio on mud weight window in the drilling of the Zagros sedimentary basin. Journal of Petroleum Geomechanics, 5(3), 26-42.

[5] Movahidnia, A. M., Qasim Al-Askari, Mohammad Kamal, and Yarahamdi, Mohsen. (2012). Estimation of optimal mud pressure using different failure criteria in deviated wells, case study: well 2sk 5 of Salman oil field. Oil Research, 23(73), 104-112. https://sid.ir/paper/114886/fa

[6] Poursiami, H. (2013). Pore pressure modeling of hydrocarbon reservoir in southwest of Iran using well logging data.

[7] Rafieipour, S., Ghotbi, C., Pishwai, M., & Jalairi, H. (2012). Well stability analysis in one of the southwestern fields of Iran The first international oil, gas, petrochemical and power plant conference, https://civilica.com/doc/158038

[8] Taherdang Kou, R., Hamiyali, H., & Zargarbashi, M. (2014). Analysis of wellbore wall stability according to rock mechanics considerations (southwest of Iran) The third scientific conference on engineering of hydrocarbon reservoirs and upstream industries, https://civilica.com/doc/265537

[9] Mirani, M., & Habibnia, B. (2014). Wellbore Stability Analysis During Drilling Using Geomechanical Model and FLAC3D Software in Asmari Reservoir, Ahwaz Oil Field. Iranian journal of petroleum Geology, 4(1), 68-. https://www.magiran.com/paper/1466230

[10] Alizadeh Saeed, P., Hasanpour Sedghi, M., & Kadkhodaei, A. (2016). Investigating the stability of the wall of oil wells with the help of STABView software Second International Congress of Earth Sciences and Urban Development, https://civilica.com/doc/526447

[11] Zain-Ul-Abedin, M., & Henk, A. (2020). Building 1D and 3D mechanical earth models for underground gas storage—A case study from the Molasse Basin, Southern Germany. Energies, 13(21), 5722.

[12] Mohammed, A. K., & Selman, N. S. (2020). Building 1D mechanical earth model for Zubair oilfield in Iraq. J Eng, 26(5).

[13] Abdulaziz, A. M., Abdulridha, H. L., Dahab, A. S. A., Alhussainy, S., & Abbas, A. K. (2021). 3D mechanical earth model for optimized wellbore stability, a case study from South of Iraq. Journal of Petroleum Exploration and Production Technology, 11(9), 3409-3420.

[14] Kidambi, T., & Kumar, G. S. (2016). Mechanical earth modeling for a vertical well drilled in a naturally fractured tight carbonate gas reservoir in the Persian Gulf. Journal of Petroleum Science and Engineering, 141, 38-51.

[15] Mursalin, M., Romario, F., Setiawan, A., Firmansyah, D., & Negara, B. J. K. (2021). Implementation of Mechanical Earth Model in Predicting the Maximum Water Injection Flow Rate in Mature Field. Jurnal IATMI.

[16] Goodman, H. E., & Connolly, P. (2007). Reconciling subsurface uncertainty with the appropriate well design using the mechanical Earth model (MEM) approach. SPE Nigeria Annual International Conference and Exhibition,

[17] Oruji, M., and Ameri Shahrabi, Javad. (2016). Determining the optimal drilling route in one of the fields of the Persian Gulf using the earth mechanical model. Oil Research, 27(95), 134-146. https://sid.ir/paper/115039/fa

[18] Zakeri Moghadam, S., Ahmadi Rad, B., & Badri, F. (2018). Providing a mechanical earth model to determine the appropriate depth for hydraulic fracture (a case study in one of the oil fields in western Iran) 3rd

National Petroleum Geomechanics Conference, https://civilica.com/doc/1031433

[19] Sharifi, J., Sekoti Diarjan, M., Ebrahimi, M., & Hafezi Moghadas, N. (2016). Presenting the mechanical earth model for geomechanical purposes using petrophysical logs The 9th Conference of Engineering Geology and Environment of Iran, https://civilica.com/doc/583065

[20] Mansouri, Y., Ameri, M. J., Kamal Qasem al-Sakri, M., & Rahimzadeh Kiwi, I. (2015). Improving the stability of the well using the mechanical earth model: (a case study in one of the fields located in the Persian Gulf) The first petroleum geomechanics conference, https://civilica.com/doc/384606

[21] Narimizadeh, L., & Abdideh, M. (2012). Analysis of reservoir rock fractures by the use of mechanical earth model (MEM) The 16th conference of the Geological Society of Iran, https://civilica.com/doc/181558

[22] McCann, D., & Entwisle, D. (1992). Determination of Young's modulus of the rock mass from geophysical well logs. Geological Society, London, Special Publications, 65(1), 317-325.

[23] Ahmadinejad, A., & Khosravanian, R. (2017). Determination of Mud Weight Window Based on Analytical and Numerical Analyses.

[24] Knöll, L. O. (2016). The process of building a mechanical earth model using well data University of Leoben].

[25] Swift, S. A., & Bower, A. S. (2003). Formation and circulation of dense water in the Persian/Arabian Gulf. Journal of Geophysical Research: Oceans, 108(C1), 4-1-4-21.

[26] Fjær, E., Holt, R., Horsrud, P., Raaen, A., & Risne, A. (2008). Petroleum related rock mechanics, Elsevier. In: Amsterdam.

[27] Zoback, M. D. (2010). Reservoir geomechanics. Cambridge university press.

[28] Khaksar, A., Taylor, P. G., Fang, Z., Kayes, T., Salazar, A., & Rahman, K. (2009). Rock strength from core and logs, where we stand and ways to go. SPE Europec featured at EAGE Conference and Exhibition?,

[29] Chang, C., Zoback, M. D., & Khaksar, A. (2006). Empirical relations between rock strength and physical properties in sedimentary rocks. Journal of Petroleum Science and Engineering, 51(3-4), 223-237.

[30] Golubev, A., & Rabinovich, G. (1976). Resultaty primeneia appartury akusticeskogo karotasa dlja predeleina proconstych svoistv gornych porod na mestorosdeniaach tverdych isjopaemych. Prikl. Geofiz. Moskva, 73, 109-116.

[31] Rahman, K., Khaksar, A., & Kayes, T. (2008). Minimizing sanding risk by optimizing well and perforation trajectory using an integrated geomechanical and passive sand-control approach. SPE Annual Technical Conference and Exhibition?,

[32] Plumb, R. (1994). Influence of composition and texture on the failure properties of clastic rocks. SPE/ISRM Rock Mechanics in Petroleum Engineering,

[33] Eaton, B. A. (1975). The equation for geopressure prediction from well logs. SPE Annual Technical Conference and Exhibition?,

[34] Zoback, M. D., Barton, C., Brudy, M., Castillo, D., Finkbeiner, T., Grollimund, B., Moos, D., Peska, P., Ward, C., & Wiprut, D. (2003). Determination of stress orientation and magnitude in deep wells. International Journal of Rock Mechanics and Mining Sciences, 40(7-8), 1049-1076.

[35] Fjaer, E., Holt, R. M., Horsrud, P., & Raaen, A. M. (2008). Petroleum related rock mechanics. Elsevier.

[36] Al-Ajmi, A. M., & Zimmerman, R. W. (2005). Relation between the Mogi and the Coulomb failure criteria. International Journal of Rock Mechanics and Mining Sciences, 42(3), 431-439.

[37] Al-Ajmi, A. (2006). Wellbore stability analysis based on a new true-triaxial failure criterion KTH].